



ARTICLE

Improvement of Cemented Gangue Backfill Material with Barium Hydroxide in Acid Mine Water

Xiaoli Ye^{1,2}, Yuxia Guo^{1,2,*}, Peng Wang^{1,2}, Yonghui Zhao^{1,2}, Wenshuo Xie^{1,2} and Guorui Feng^{1,2}

¹College of Mining Technology, Taiyuan University of Technology, Taiyuan, 030024, China

²Province Coal-Based Resources Green and High-Efficiency Development Engineering Center, Taiyuan, 030024, China

*Corresponding Author: Yuxia Guo. Email: gyx771221@163.com

Received: 30 April 2022 Accepted: 14 June 2022

ABSTRACT

As a kind of green concrete, the mechanical properties and durability of cemented gangue backfill material (CGBM) will be affected if they are in acid mine water with sulfate ions in the long term. To improve the performance of CGBM in acid mine water with sulfate ions, CGBM specimens with different doses of barium hydroxide were immersed in sulfuric acid solutions of different concentrations for 270 days. The changes of mass, ultrasonic pulse velocity (UPV) and compressive strength of the specimens at different ages were analyzed. Scanning electron microscopy (SEM) and X-ray diffraction (XRD) were used to analyze the microstructure and composition of the specimens. The results show that incorporation of barium hydroxide into CGBM specimen can promote the formation of barium sulfate precipitation and inhibit the generation of corrosion products such as ettringite. Meanwhile, barium sulfate precipitation blocks the pore channel invaded by sulfuric acid solution, delaying the progress of corrosion reaction and making the interior of CGBM specimen more complete. And the specimen with 2.0 kg/m³ barium hydroxide was more effective in improving performance. This study provides a basis for the ratio design of CGBM in acid mine water with sulfate ions.

KEYWORDS

Cemented gangue backfill material; sulfate ions; corrosion; barium hydroxide; microscopic performance; deterioration mechanism

1 Introduction

Coal resources as an important raw material for power generation and chemical production, greatly promote the development of the industry and world economy [1]. As a kind of solid waste generated in coal production and processing, coal gangue has a continuous increase in production and an increasingly arduous task of governance, resulting in an increasingly heavy economic and environmental burden on enterprises and surrounding areas [2,3]. The treatment and utilization of coal gangue have become a prominent problem in the development process of many coal enterprises. The cemented gangue backfill material (CGBM) is used to backfill the coal mine goaf, which improves the utilization rate of mineral resources and realizes the sustainable development of resources [4]. CGBM for backfill mining is prepared by gangue, cement, fly ash and water. Due to the high cost of cement and fly ash compared with other raw materials, the application of full backfill mining technology based on CGBM in coal mines is



restricted. Therefore, in order to reduce the cost of backfill mining, relevant scholars have proposed constructional backfill mining technology [5–7], which is supported by filling strips or filling pillars in the form of CGBM to control surface subsidence and ensure safe mining. If the filling strip or filling pillars with structural function is in a complex goaf environment, such as a corrosive mine water environment, the long-term mechanical and deformation properties of the cemented paste backfill will change. In severe cases, it will lead to instability and failure of the cemented paste backfill, and then affect the stability of the roof.

Underground coal mines often contain a large amount of mine water with complex components [8]. By investigating the composition of mine water in 37 measuring points of 12 mining areas in Shanxi, China, it is known that most of the mine water in Shanxi Province contains SO_4^{2-} , HCO_3^- , Cl^- , Mg^{2+} , Na^+ , Ca^{2+} , of which the content of SO_4^{2-} and HCO_3^- are more, and the pH value of mine water is between 2.63 and 8.75. The pH value of mine water in some mines is less than 7. As a cement-based material, CGBM is alkaline after hydration reaction. When the cemented paste backfill is in acid mine water containing sulfate ions for a long time, corrosive ions will enter the CGBM and undergo a chemical reaction [9,10], generating a large amount of soluble salt to fill the internal pores of CGBM. When the salts leached from CGBM, the porosity of CGBM increases and the pH value of the pore solution decreases, which makes the internal structure of the cemented paste backfill gradually loose [11–17]. In serious cases, it will lead to the instability and damage of the cemented paste backfill, which will affect the stability of the roof. Based on the above, it is necessary to propose corresponding improvement measures according to the environment to improve the performance of CGBM and ensure the safety and stability of cemented paste backfill in structural backfill mining.

Due to the deterioration of cement-based materials in a sulfuric acid environment, scholars have put forward various improvement measures to improve the corrosion resistance of cement-based materials in a sulfuric acid environment. A very popular strategy used to improve the sulfuric acid resistance of cement-based materials is to add admixtures. Some studies use pozzolanic substances, including fly ash, slag, silica fume, etc. [18–20]. Said et al. [21] studied the effect of adding natural volcanic ash and limestone on the sulfuric acid corrosion resistance of self-compacting concrete. The results show that the self-compacting concrete with natural pozzolana will have a pozzolanic reaction, which increases the content of C-S-H and improves the pore structure of self-compacting concrete. Therefore, it showed good corrosion resistance in sulfuric acid, while the corrosion resistance of self-compacting concrete with limestone was lower than that of ordinary vibrated concrete. The pore structure of this kind of cement-based materials were improved and the porosity was small, so as to reduce the transmission speed of sulfate ions in cement-based materials. And the interface transition zone between cement and aggregate was improved, which enhanced the durability of cement-based materials. Another strategy to enhance the resistance to sulfuric acid corrosion is the use of aggregates derived from polymers or ceramic in cement-based materials. Araghi et al. [22] used PET (Polyterephthalate) to replace the aggregate in concrete to increase the sulfuric acid corrosion resistance of concrete. By testing the size change, strength loss, mass loss and UPV of specimens at different ages, the results show that the sulfuric acid resistance of concrete was the best when the substitution rate was 15%. This kind of cement-based material had low permeability, and had lower mass loss and crushing load loss than ordinary concrete in a sulfuric acid environment, therefore it showed good sulfuric acid resistance.

The addition of additives can also effectively improve the internal structure of cement-based materials so as to improve the sulfuric acid resistance [23,24]. Yang et al. [25] improved the reactivity of calcium hydroxide activated slag mortar by adding barium hydroxide. The research showed that adding barium hydroxide helped to form C-S-H gel with long-term stability. The gel had a higher molar ratio of silicon to calcium, which improved the durability of mortar and maintained long-term high strength. Mobasher et al. [26] added barium hydroxide to the blast furnace slag cement composite to slow down the corrosion

reaction. The results showed that barium hydroxide formed a highly cross-linked C-A-S-H gel in the hydration reaction, which fixed sulfate ions in the corrosion solution. Wang et al. [27] studied the effect of polycarboxylate superplasticizer on the corrosion resistance ion penetration of concrete. It was found that with the decrease of the length of PCE side chain, the adsorption capacity and adsorption layer thickness of PCE increased, the absolute zeta potential of cement increased, and the initial hydration was delayed, resulting in fewer micro-cracks in concrete. García-Vera et al. [28] analyzed the compressive strength, UPV, and mass loss of cement-based materials mixed with crystal admixtures after 90 days of exposure in sulfuric acid environment. They pointed out that the crystal admixtures blocked the pores, capillary channels and microcracks and prevented the penetration of external sulfuric acid solution. Therefore, cement-based materials containing crystal admixtures showed higher compressive strength and lower mass loss than those without crystal admixtures.

In this study, different doses of barium hydroxide reagents were added into CGBM to improve the corrosion resistance of CGBM in acid mine water with sulfate ions. By measuring the mass, UPV and compressive strength of CGBM specimens under different conditions, and analyzing the microstructure and chemical compositions of specimens after corrosion, the effect of adding different doses of barium hydroxide on improving the performance of CGBM in acid mine water with sulfate ions was characterized. This study can provide reference for the design of cemented paste backfill in constructional backfill mining.

2 Experimental Program

2.1 Raw Material

2.1.1 Cement

The cement was 42.5 ordinary Portland cement produced by Taiyuan Shitou Cement Co., Ltd., China. The main chemical composition is shown in Table 1, and the scanning electron microscope microstructure (SEM) and X-ray diffraction (XRD) patterns are shown in Fig. 1a. The initial setting time and final setting time of cement are 160 min and 220 min, respectively. The compressive strength of this grade cement for 3 days and 28 days is 17.4 MPa and 45.4 MPa, respectively. The particle size distribution of cement is shown in Fig. 2a.

Table 1: Chemical component of raw material

Chemical components	Cement (%)	Fly ash (%)	Coal gangue (%)
SiO ₂	22.36	52.42	35.46
Al ₂ O ₃	5.53	32.48	16.11
Fe ₂ O ₃	3.46	3.62	3.86
CaO	65.08	0.99	7.15
MgO	2.1	1.01	3.50
TiO ₂	—	1.26	0.80
Others	1.47	8.22	33.12
Fineness (>45 μm) (%)	5	42.54	53.78

2.1.2 Fly Ash

Fly ash was grade II fly ash produced by Taiyuan Jinyang Fly Ash Comprehensive Utilization Co., Ltd., China. The main chemical composition is shown in Table 1, and the SEM and XRD patterns are shown in Fig. 1b. The content of Cao in the test fly ash is less than 10%, which belongs to low calcium fly ash. More than 80% of fly ash is composed of SiO₂ and Al₂O₃. SiO₂ and Al₂O₃ provide the main activity of fly ash. The particle size distribution of fly ash is shown in Fig. 2b.

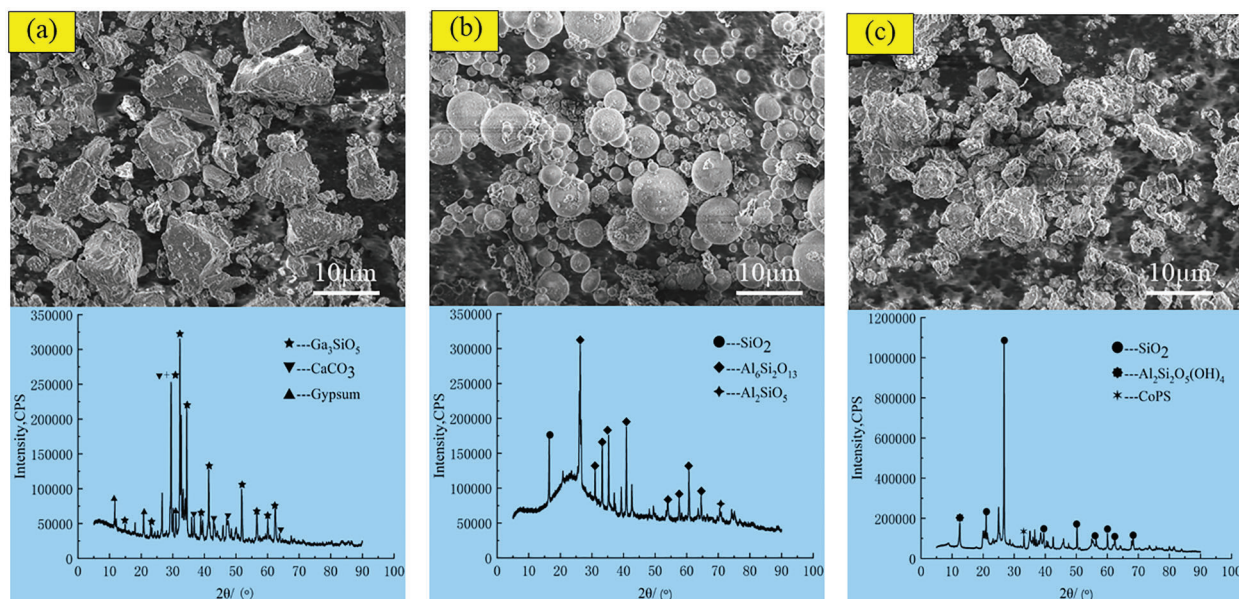


Figure 1: SEM and XRD spectrums of raw materials. (a) Cement (b) Fly ash (c) Coal gangue

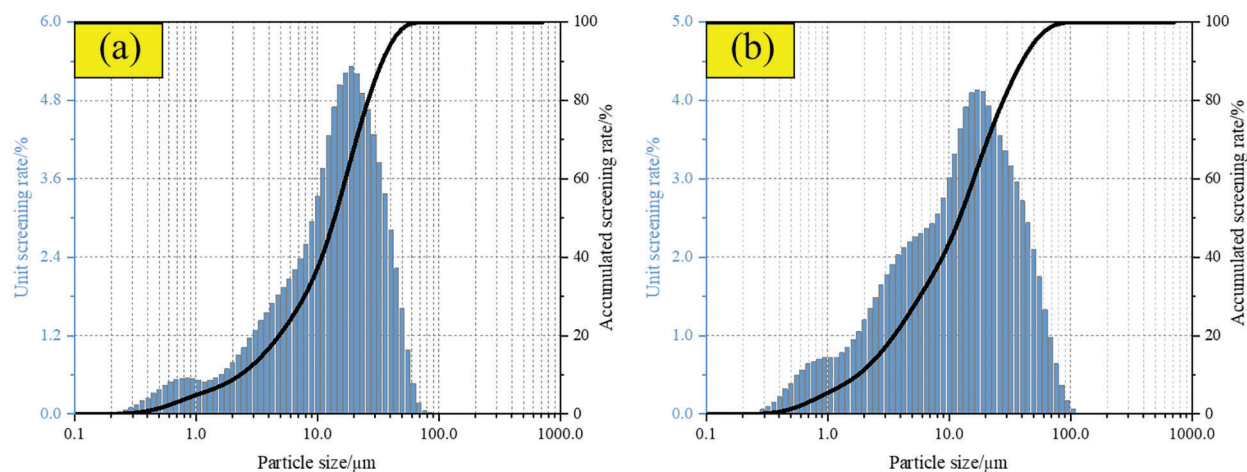


Figure 2: Particle size distribution. (a) Cement (b) Fly ash

2.1.3 Coal Gangue

Coal gangue was collected from Tunlan Coal Mine, Shanxi Province, China. It was broken and screened into fine aggregate with a particle size of 0–5 mm and coarse aggregate with a particle size of 5–15 mm [29–31]. Its apparent density is 2900 kg/m^3 . The main chemical composition is shown in Table 1, and the SEM and XRD patterns are shown in Fig. 1c.

2.1.4 Barium Hydroxide and Stirring Water

The barium hydroxide reagent is AR grade analytical pure reagent produced by Shandong Xiya Chemical Technology Co., Ltd., China. The pure reagent barium hydroxide has a relative molecular weight of 171.34 and is soluble in water and ethanol. Tap water was used as stirring water.

2.2 Mix Design and Specimen Preparation

The basic mix proportion of CGBM and the mixing proportion of different doses of barium hydroxide are given in Table 2 (“kg/m³” means the weight of each material per cubic meter of specimen). After the raw material was fully mixed, the fresh CGBM was poured into the cube molds of 100 mm × 100 mm × 100 mm, the bubbles were removed by vibration for 1 min, and the plastic film was covered. After pouring for 24 h, the specimens were demoulded and maintained at 20 ± 2°C and 98% relative humidity for 28 days accordant to ASTM C192 [32]. A total of 180 specimens were prepared.

Table 2: Mix design of CGBM

No.	Unit weight (kg/m ³)					
	Cement	Fly ash	Gangue aggregate		Water	Ba(OH) ₂
			0–5 mm	5–15 mm		
K0	190	380	285	665	380	0
K1						1.6
K2						1.8
K3						2.0
K4						2.2

2.3 Experimental Procedure

Through the investigation of mine water composition at 37 measuring points in 12 mining areas in Shanxi Province, it is determined that the corrosive medium can be a sulfuric acid solution with pH = 3 and 5. The specific experimental process is presented in Fig. 3. The specimens cured for 28 days were immersed in sulfuric acid solutions with different pH values for 30, 60, 90, 180 and 270 days, respectively. Replaced the sulfuric acid solution periodically to keep the pH value of the solution basically unchanged until the desired immersion time was reached. After taking out the CGBM specimens from the solution, the specimens were washed twice with distilled water to remove the loose reaction products, and then the water on the surface of the specimens was wiped clean. After that, dry the specimens for one hour before measuring mass, UPV and compressive strength. The specimens' mass was weighed by an electronic balance with a precision of 100 mg. UPV was monitored by NM-4B non-metallic ultrasonic testing analyzer. The compressive strength was measured by YAW-200B micro-controlled electronic pressure testing machine. The specimens with 2.0 kg/m³ barium hydroxide and the control specimens with soaking time of 60, 180 and 270 days were taken to prepare the powder of the sample. JSM-7001F thermal field emission scanning electron microscope was used to observe and analyze the microstructure of SEM, and the chemical composition was analyzed by XRD test with Ultima IV multipurpose X-ray diffraction system.

3 Results and Discussion

3.1 Mass

After immersion in sulfuric acid solution, the surface of the CGBM specimen would be loose and damaged to a certain extent. Therefore, the acid corrosion failure process of the material could be reflected by measuring the mass change of the specimen. The relationships between the mass of CGBM specimen with different barium hydroxide and immersion time are presented in Fig. 4. It can be observed that the mass of control specimens declined first, then increased and then decreased with the increase of immersion age. This phenomenon may be caused by the fact that calcium hydroxide specimen combined

with H^+ to generate water and continuously dissolved, which reduced the mass of the specimen in the early age. With the product generated by cement hydration, the mass of the specimen increased. Then the alkaline environment in the specimen was destroyed, and the hydration product continuously dissolved, leading to the continuous decrease of the mass of the specimen in the later age. After 270 days, the mass of control specimens was 1949 g and 1952 g, which increased by 0.05% and 0.21% compared with the initial mass for pH = 3 and 5, respectively. Kumar et al. [33] studied the durability of geopolymer concrete soaked in 5% sulfuric acid solution for 24 weeks, and concluded that the mass of the specimen increased in early age, and mass began to decrease after 12 weeks. This is consistent with the variation of specimen mass in this paper.

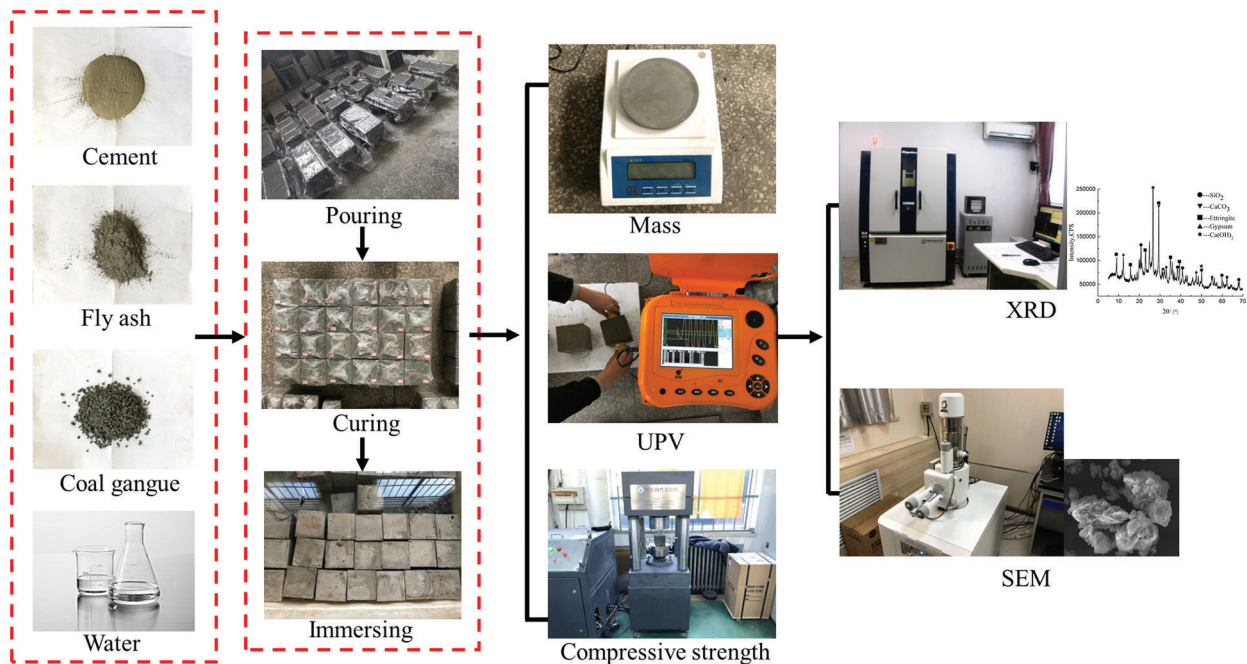


Figure 3: Experimental procedure

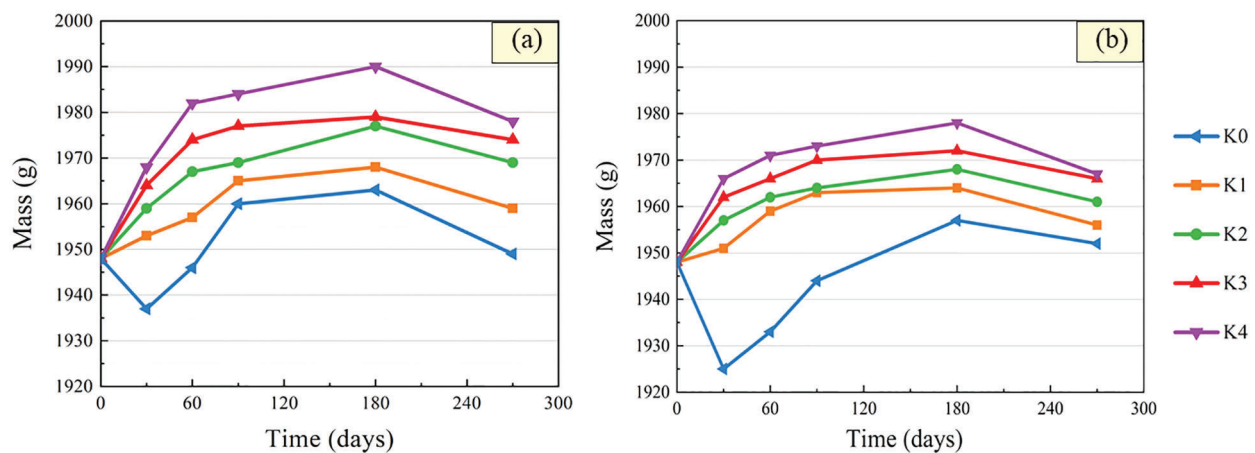


Figure 4: Mass variation after immersion in sulfuric acid solution. (a) pH = 3 (b) pH = 5

With the increase of immersion time, the mass of specimen with barium hydroxide increased first and then decreased, and the change trend gradually slowed down. The smaller the pH value of sulfuric acid solution, the more obvious the change of specimen quality. Compared with the control sample, the change of mass with the soaking age of the specimen with barium hydroxide was less than a decline stage (0–30 days). It is possible that the mass of BaSO_4 generated in the early age is greater than that of dissolved water. At 180 days, the mass of CGBM sample in sulfuric acid solution with pH=3 and 5 began to decrease obviously. After soaking in sulfuric acid solution with pH=3 for 270 days, the mass of specimens with 1.6, 1.8, 2.0, 2.2 kg/m^3 barium hydroxide decreased by 0.56%, 1.08%, 1.33% and 1.54% respectively compared with peak mass. In the solution with pH=5, the mass of specimens with each dose decreased by 0.41%, 0.67%, 0.92% and 0.98% respectively compared with peak mass. It can be seen that the mass of specimens increased with the increase of barium hydroxide content in all immersion ages. And the mass of the specimen with 2.0 kg/m^3 barium hydroxide changed the most slightly. This shows that the addition of barium hydroxide could delay the corrosion reaction to a certain extent and alleviate the formation of corrosion products.

3.2 UPV

Ultrasonic testing technology is mainly used to indirectly reflect the structural characteristics of the material medium through the parameters such as the propagation speed, frequency and amplitude of ultrasonic in the medium. Because of its simplicity, accuracy and non-destructive testing, ultrasonic testing technology has great advantages in the research of damage detection of cement-based materials [34–38]. The variation curves of UPV with time after immersion of CGBM specimens with different barium hydroxide are demonstrated in Fig. 5. It can be found that the UPV of control specimens increased first and then decreased. At 90 days, the mass of CGBM specimens in sulfuric acid solution with pH=3 and 5 began to decrease obviously. This is because the hydration products generated by the hydration reaction in the early age of the specimen filled the interior of the specimen, making the specimen more compact. However, with the increase of soaking age, the hydration products dissolved slowly, and the internal porosity of the specimen increased, resulting in the decrease of UPV after 90 days. This phenomenon is similar to the variation of concrete UPV within 150 days of erosion age studied by Pang et al. [39].

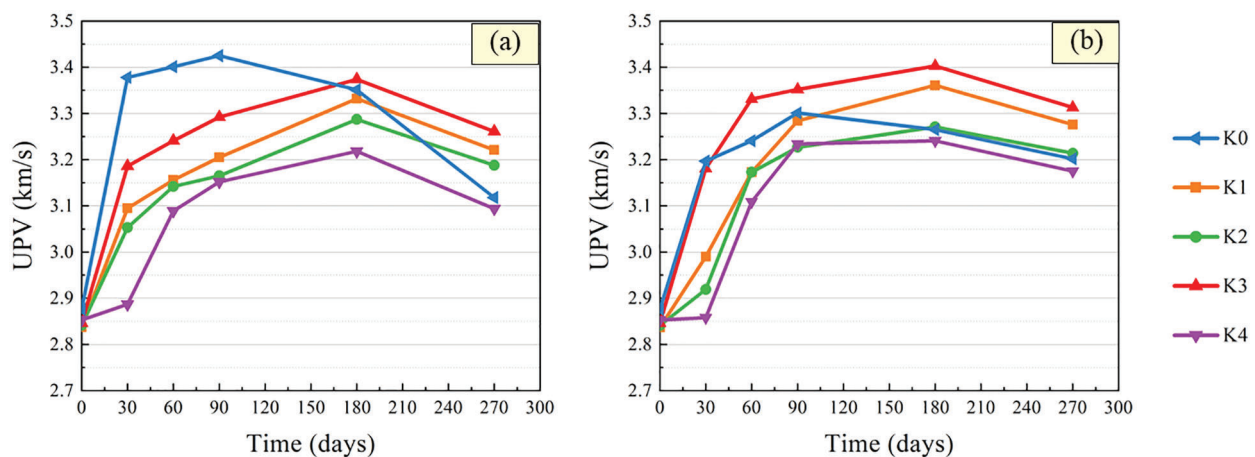


Figure 5: UPV variation after immersion in sulfuric acid solution. (a) pH = 3 (b) pH = 5

The UPV of specimens with barium hydroxide also showed a trend of increasing first and then decreasing. However, UPV began to decrease after the immersed for 180 days, which was delayed compared with the control specimen. The smaller the pH value of sulfuric acid solution was, the more the UPV of the specimen with barium hydroxide was increased and the more the decrease was. It can be seen

that the UPV of the specimen with 2.0 kg/m^3 barium hydroxide was the largest and that of the specimen with 2.2 kg/m^3 barium hydroxide was the smallest. From 180 days to 270 days, the UPV of the specimens with barium hydroxide decreased more slowly than that of the control specimens. This shows that the addition of an appropriate amount of barium hydroxide improved the internal structure of CGBM specimens, thereby reducing the diffusion of corrosive ions, thus improving the compactness of the specimens.

3.3 Compressive Strength

The variation curves of compressive strength with time of specimens with different barium hydroxide are given in Fig. 6. It can be seen that the compressive strength of the control specimens after immersion increased first and then decreased. This is basically consistent with the change trend of UPV with soaking age. After immersion in solutions with pH=3 and 5, the peak compressive strength of the control specimens appeared for 90 days, which means that the compressive strength of the control specimens began to decrease at 90 days. At 270 days, the compressive strength of control specimens was 9.03 and 10.21 MPa, respectively, which was 40.7% and 18.9% lower than that at 90 days. The results show that the smaller the pH value of the solution, the more obvious the change of compressive strength of the control specimen.

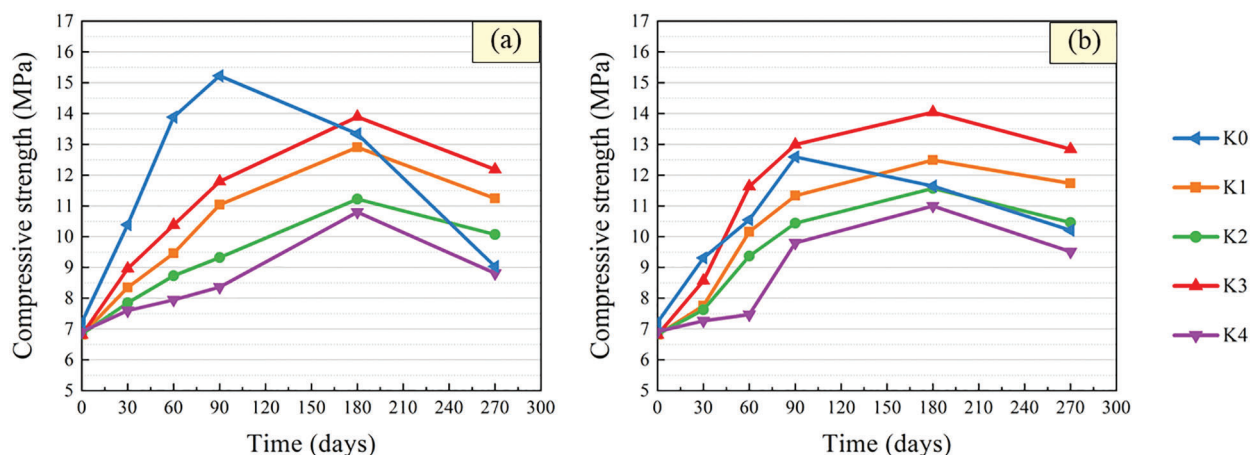


Figure 6: Compressive strength variation after immersion in sulfuric acid solution. (a) pH = 3 (b) pH = 5

The compressive strength of specimens with barium hydroxide also showed a trend of increasing first and then decreasing, as shown in Fig. 6. After 180 days of immersion, the strength of the specimen with barium hydroxide began to show a downward trend, which was later than that of the control specimen. This is consistent with the variation of compressive strength of specimens within 2 months of erosion age after adding barium hydroxide into tuff sand concrete studied by Xiao et al. [40]. And the smaller the pH value of the solution, the more significant the change of the compressive strength of the specimen mixed with barium hydroxide. This is because the concentration of corrosive ions increased, which accelerated the corrosion rate of specimens in pH=3 solution. After 270 days of immersion in sulfuric acid with pH=3 and 5, the strength of specimens with 1.6, 1.8 and 2.0 kg/m^3 barium hydroxide were higher than that of control specimens. The strength of specimens with 2.0 kg/m^3 barium hydroxide was the highest and the strength of specimens immersed in sulfuric acid solution with pH=3 and 5 for 270 days increased by 78.85% and 88.55% compared with the initial strength, respectively. It can be seen that addition of barium hydroxide can delay the corrosion reaction of CGBM specimens in the sulfuric acid corrosion environment, and the effect of adding 2.0 kg/m^3 barium hydroxide was the best. Jeong et al. [41] believe that barium ions and sulfate ions generate BaSO_4 , thus reducing ettringite, and the existence of ettringite can increase the early strength, which is in accordance with the phenomenon that the early strength of specimen with barium hydroxide is less than that of control specimen in this paper.

3.4 Compressive Strength–UPV Relationships

Due to compressive strength is related with elastic modulus, and UPV is related with elastic modulus and material density [42,43], there is a certain relationship between UPV and compressive strength. Nematzadeh et al. [19] studied the relationship between the compressive strength and UPV of concrete specimens containing forta-ferro fibers, and used the exponential function to determine the relationship between the compressive strength and UPV. Bogas et al. [44] used UPV to predict the compressive strength of lightweight aggregate concrete, put forward the exponential expression of UPV and compressive strength, and obtained a high correlation coefficient. These results show that the relationship between compressive strength and UPV can be expressed by exponential function as Eq. (1):

$$F'_c = A \cdot e^{(BV)} \tag{1}$$

where F'_c and V are compressive strength (MPa) and UPV (km/s) of cement-based materials, respectively, and coefficients A and B are empirical constants. Through the nonlinear regression analysis of the experimental data, the empirical constants A and B are obtained, so as to determine the relationships between the compressive strength and UPV of CGBM specimens with barium hydroxide content of 0, 1.6, 1.8, 2.0 and 2.2 kg/m³. The empirical relationships between compressive strength and UPV of CGBM specimens with different barium hydroxide doses are presented in Fig. 7.

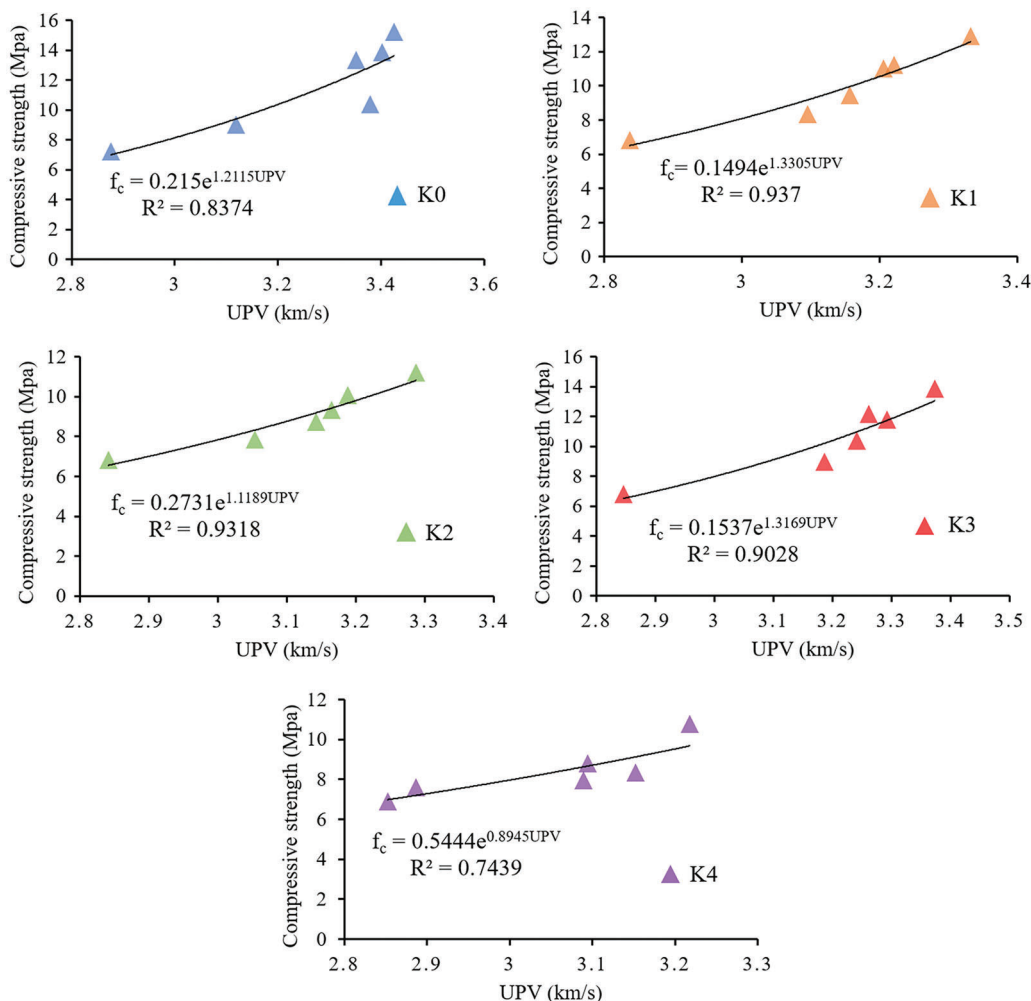


Figure 7: Non-linear regression analysis of UPV and compressive strength

3.5 SEM and XRD

In order to reveal the mechanism of acid corrosion and the effect of barium hydroxide on the degradation of CGBM, the micro morphology and phase composition of the materials were observed by SEM and XRD. Figs. 8 and 9 display the SEM and XRD patterns of the control specimen and specimen with 2.0 kg/m^3 barium hydroxide immersed in sulfuric acid solution with $\text{pH} = 3$. Fig. 8a shows that short villous crystals began to appear after 60 days of corrosion. It can be observed that the diffraction peaks of ettringite in the XRD pattern appeared near the diffraction angles of 10° , 30° and 42° , and there were gypsum diffraction peaks with low intensity near 12° , 45° and 55° . A large number of disordered coarse acicular ettringite crystals and a small amount of flocculent C-S-H were observed in the 180-day control specimen (Fig. 8b). In the corresponding XRD patterns, it is found that the diffraction peaks of ettringite and gypsum in the control specimens increased relatively, and the intensity of the diffraction peaks of ettringite significantly enhanced near 30° – 50° . The diffraction peaks of gypsum with high intensity appeared near 30° and 40° , and the intensity of the diffraction peak of calcium hydroxide near 25° was obviously weakened. It is observed in Fig. 8c that at 270 days, there is only a small amount of acicular ettringite appeared in the control specimen, and the flocculent C-S-H also decreased apparently. The diffraction peak of ettringite in the corresponding XRD pattern decreased, while the diffraction peak of gypsum increased obviously. The diffraction peak intensity of ettringite around 30° and 45° weakened, and the diffraction peak intensity of gypsum around 21° , 27° and 35° increased significantly. At 60 days, the SEM morphology of the specimen with barium hydroxide (Fig. 9a) had no obvious difference compared with that of Fig. 8a, and the unreacted fly ash particles were found. Correspondingly, the diffraction peak intensities of ettringite and gypsum in the XRD pattern (Fig. 9a) were not visibly different from those of the control specimen. While the diffraction peak intensities of calcium hydroxide near 50° were higher than those of the control specimen, because the addition of barium hydroxide increased OH^- . Compared with Fig. 8b, it can be seen that the needle-like ettringite in the 180 days specimen with barium hydroxide (Fig. 9b) was reduced markedly. The diffraction peak intensity of ettringite with diffraction angle of 35° in the XRD pattern in Fig. 9b was apparently lower than that in Fig. 8b, indicating that the incorporation of barium hydroxide inhibited the formation of ettringite. Compared with Fig. 8c, the specimen with barium hydroxide had almost no gypsum crystals and less acicular ettringite at 270 days (Fig. 9c). Correspondingly, the intensities of ettringite diffraction peaks near 20° and 12° and gypsum diffraction peaks near 30° and 25° in the XRD pattern of Fig. 9c were lower than those in Fig. 8c. This indicated that the addition of barium hydroxide also inhibited the formation of corrosion products such as gypsum.

Figs. 10 and 11 show the SEM morphology and XRD phase components of the control specimen and the specimen with 2.0 kg/m^3 barium hydroxide specimen corroded in sulfuric acid solution with $\text{pH} = 5$. Compared with Figs. 8a and 10a had only a small number of fluffy crystals and found fly ash particles that did not participate in the reaction. In the 180-day control specimen (Fig. 10b), compared with Fig. 8b, the needle-like ettringite crystals with cross-growth were observed, which were relatively thin, short and dense. In 270-day control specimens (Fig. 10c), flocculent C-S-H and acicular ettringite crystals were also obviously reduced compared with Fig. 8c. When the specimen with barium hydroxide was immersed for 60 days (Fig. 11a), the overall morphology and phase composition did not change significantly compared with Fig. 10a. Compared with Fig. 10b, a large amount of acicular ettringite did not occur in Fig. 11b and the intensity of ettringite diffraction peak near 40° was weakened in the XRD pattern of Fig. 11b. At 270 days (Fig. 11c), compared with Fig. 10c, there was relatively less plate gypsum. The diffraction peak intensity of gypsum near 22° became weak, and the diffraction peak intensity of ettringite near 30° also became weak. The above studies show that in sulfuric acid solutions with $\text{pH} = 3$ and 5, the corrosion products of the specimens with barium hydroxide are less than those of the control specimens, and the greater the pH value is, the less the corrosion products generated after

immersion. Karatasios et al. [45] showed that under the condition of simulated acid rain, adding barium hydroxide to lime-based concrete can make the concrete form a BaSO_4 protective layer, thus improving its durability against sulfuric acid corrosion.

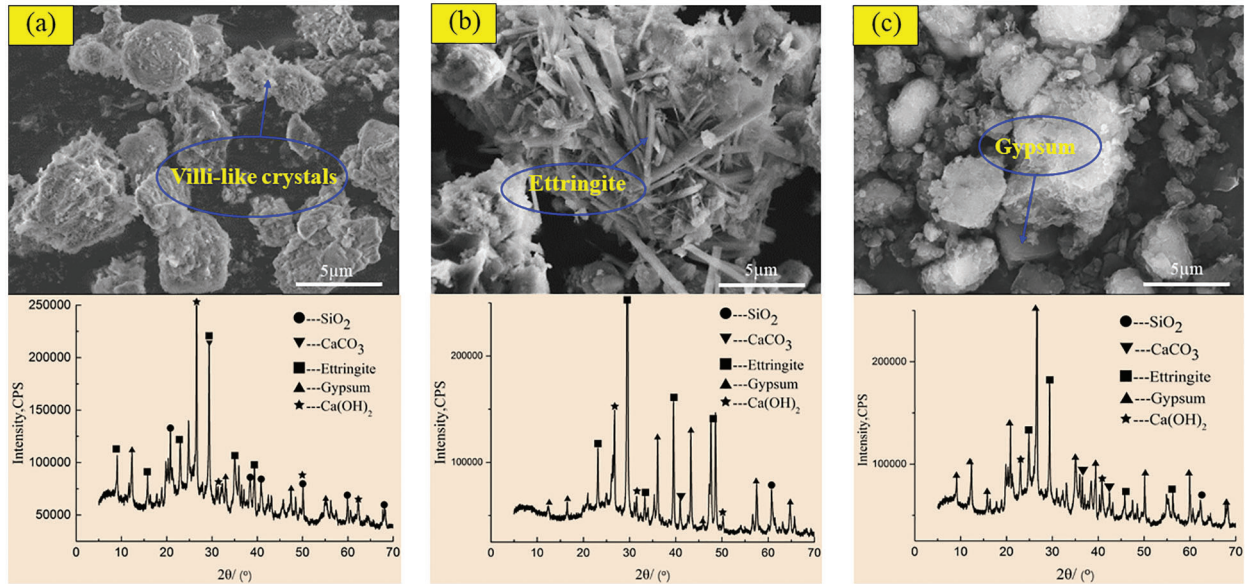


Figure 8: SEM-XRD analysis of control specimens after corrosion in sulfuric acid solution at pH = 3. (a) Control specimens for 60 days (b) control specimens for 180 days (c) Control specimens for 270 days

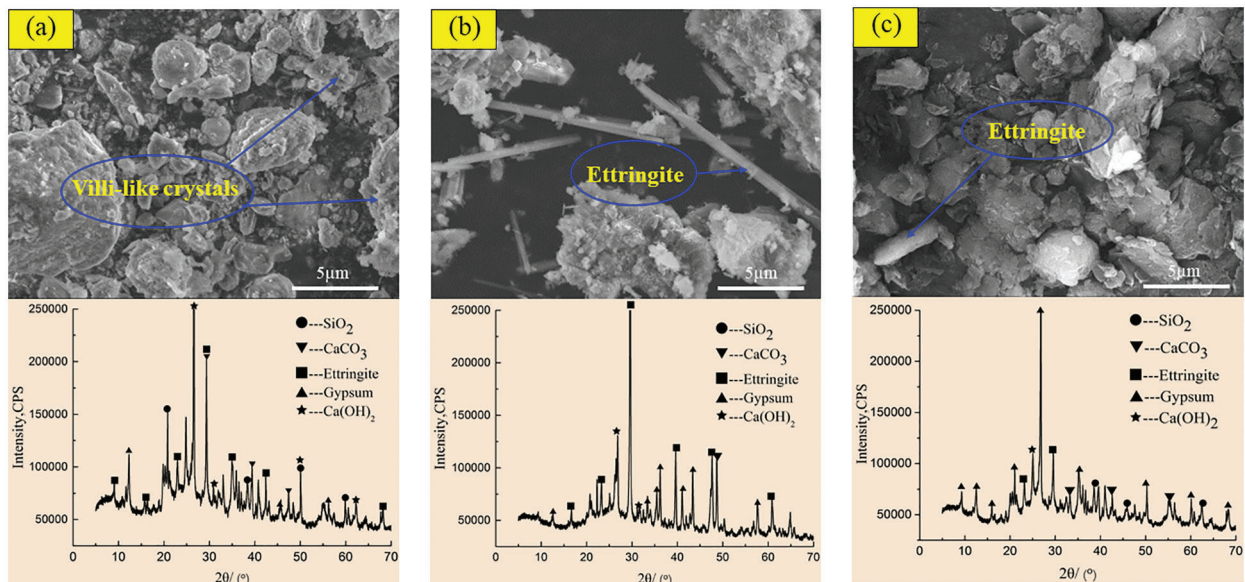


Figure 9: SEM-XRD analysis of incorporated specimens after corrosion in sulfuric acid solution at pH = 3. (a) Incorporated specimens for 60 days (b) Incorporated specimens for 18 days (c) Incorporated specimens for 270 days

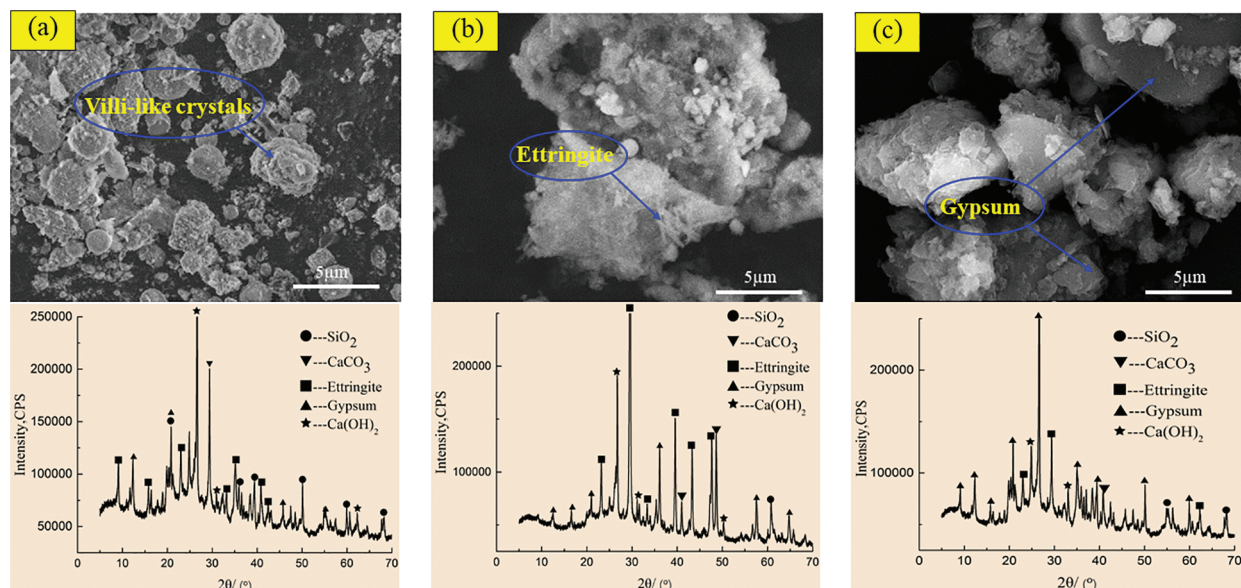


Figure 10: SEM-XRD analysis of control specimens after corrosion in sulfuric acid solution at pH = 5. (a) Control specimens for 60 days (b) Control specimens for 180 days (c) Control specimens for 270 days

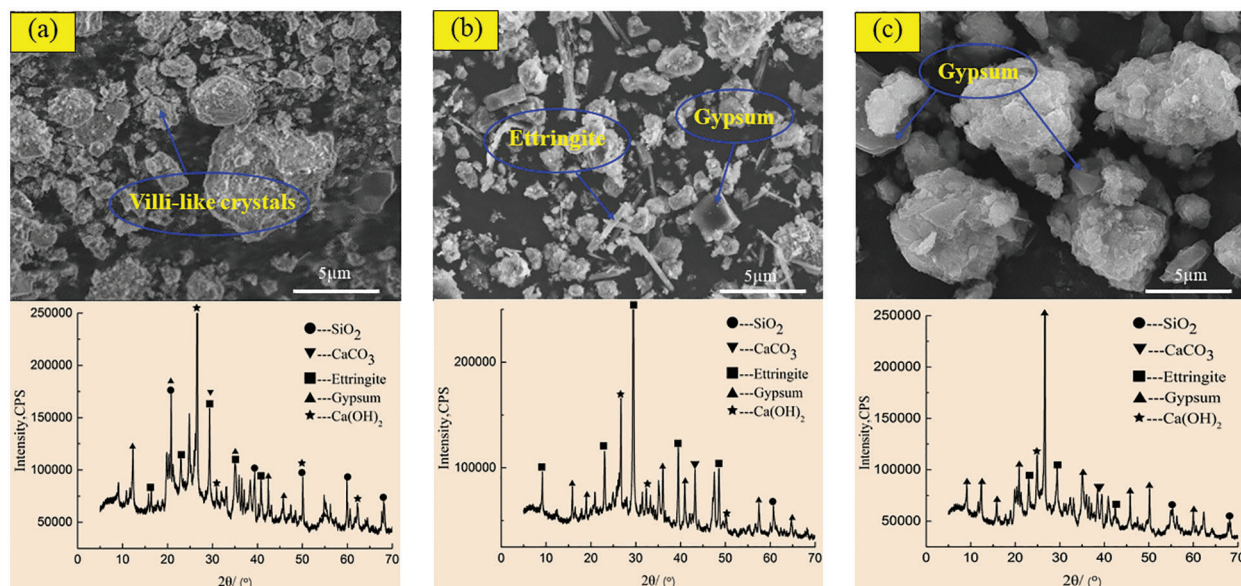


Figure 11: SEM-XRD analysis of incorporated specimens after corrosion in sulfuric acid solution at pH = 5. (a) Incorporated specimens for 60 days (b) Incorporated specimens for 180 days (c) Incorporated specimens for 270 days

3.6 Mechanism Analysis

Based on the above analysis, the main reaction process of CGBM in sulfuric acid solution is presented in Fig. 12. H^+ was neutralized with calcium hydroxide on the surface of the specimen generating water and continuously dissolved out. SO_4^{2-} diffused into the specimen and reacted with calcium hydroxide and alumina. The reaction process is given in Eq. (2). The ettringite formed by the above reaction filled the

pores in the specimen and increased the density of the specimen. Therefore, the strength and UPV of the control specimen increased from 0 to 30 days. However, at the initial stage of the reaction, the mass of the dissolved substance was greater than that of the product generated in the specimen, which was manifested as the decrease of the mass of the control specimen during the immersion period of 0–30 days. With the progress of the reaction, free Ca^{2+} generated after the neutralization reaction reacted with SO_4^{2-} and water to form gypsum dihydrate, and the reaction process is shown in Eq. (3). The hydration reaction of ordinary Portland cement produces C-S-H gel, as illustrated in Eq. (4). C-S-H gel and hydration products blocked the internal pores of the CGBM specimen and increased the compactness of the specimen. Therefore, the mass, UPV and compressive strength of the control specimen immersed for 30–90 days increased. Ettringite is relatively stable in the alkaline environment [46]. Therefore, the gradual decrease of alkalinity in the specimen would lead to the decomposition of ettringite, and the C-S-H gel would also gradually dissolve, as demonstrated in Eqs. (5) and (6), which was corresponding to the decrease in the number of ettringite crystals shown in Figs. 8b and 10b. The free Ca^{2+} produced by ettringite decomposition and SO_4^{2-} in sulfuric acid solution would form dihydrate gypsum, so the mass of the specimen continued to increase. However, because the dissolution of hydrated calcium silicate gel destroyed the cementation between it and aggregate, the strength and UPV of 90–180 days decreased. From 180 days to 270 days, the alkaline environment in the specimen was destroyed. A large amount of ettringite decomposed and dissolved after losing the survival environment, which corresponded to the continuous reduction of the number of ettringite crystals presented in Figs. 8c and 10c. Dihydrate gypsum was continuously generated and crystallized in the pores, resulting in large expansion stress, which destroyed the internal structure of the specimen, and further reduced the mass, UPV and compressive strength of the specimen [47].

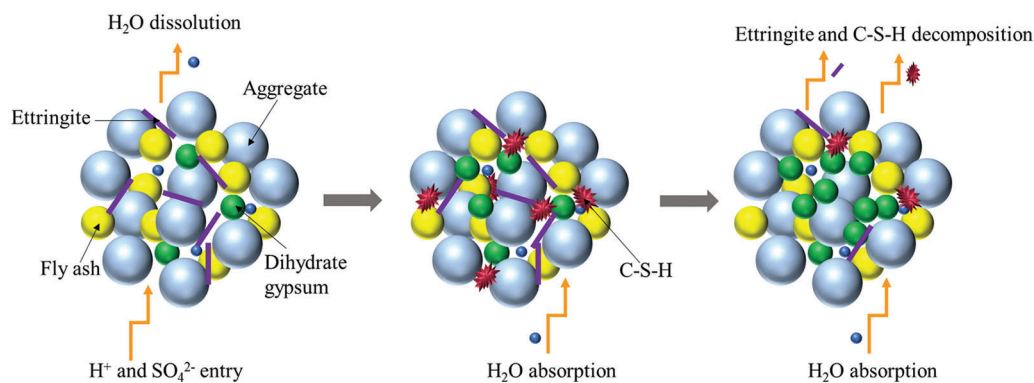
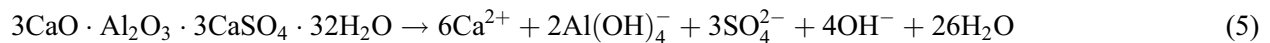
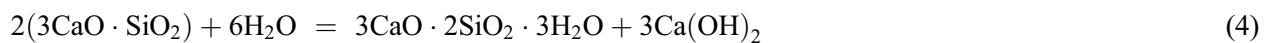


Figure 12: Reaction mechanism diagram

It can be seen from Fig. 13 that pores caused by sulfuric acid corrosion appear on the surface of the specimens. The surface of the specimen with barium hydroxide is relatively more complete, and a large

number of white precipitates are formed on the surface. The white precipitate is the barium sulfate precipitate generated by the reaction of Ba^{2+} with SO_4^{2-} , as illustrated in Eq. (7). Thus, it can be obtained that the addition of appropriate amount of barium hydroxide can not only fix sulfate ions to slow down the corrosion reaction, but also the barium sulfate precipitation can fill the pores of the specimen to increase its compactness. These two factors delay the diffusion of SO_4^{2-} in the external solution to the specimen for corrosion reaction. Therefore, in the soaking period of 0–270 days, the mass of specimens with barium hydroxide was always greater than that of control specimens. In addition, the addition of appropriate amount of barium hydroxide increased the OH^- content in the specimen and maintained the alkaline environment in the specimen. When SO_4^{2-} diffused into the specimen, the reaction of Eqs. (2) and (7) occurred, but the precipitation reaction Eq. (7) gave priority to the reaction. Therefore, the presence of barium hydroxide inhibited the formation of ettringite. And the higher the pH value is, the more obvious the inhibition is. By comparing Figs. 8c with 9c and 10c with 11c, it is also confirmed that the ettringite was greatly reduced. Therefore, at the beginning of the reaction (0–180 days), compared with the control specimen, the filling effect of ettringite in the pores of the specimen with barium hydroxide was weakened, resulting in the lower strength and UPV of the specimen with barium hydroxide than that of the control specimen. After 180 days of immersion, the internal alkaline environment of the specimen with barium hydroxide was protected, and the decreasing trend of strength and UPV was slower than that of the control specimen. The strength and UPV of the specimen with 2.0 kg/m^3 barium hydroxide were the largest and the improvement effect was the most significant.

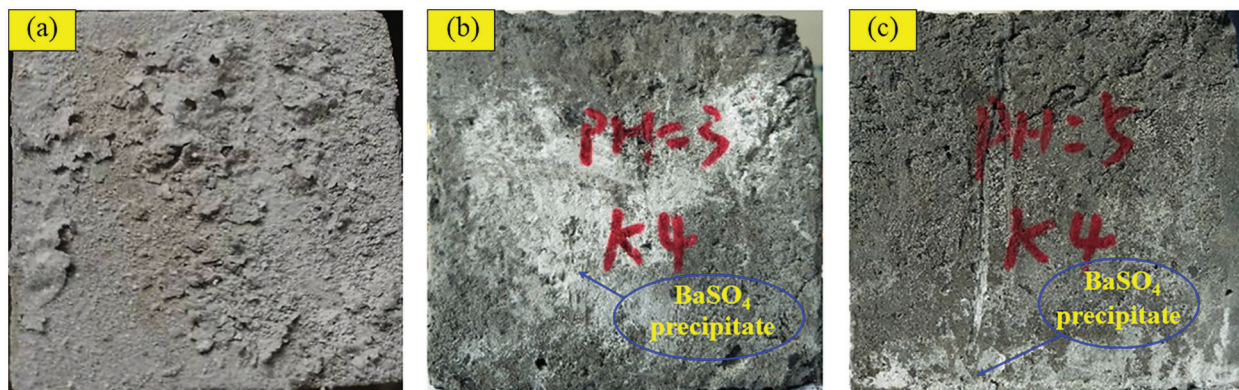


Figure 13: Appearance of control specimens and specimen with barium hydroxide at the age of 180-day. (a) Control specimen (b) pH = 3, K4 (c) pH = 5, K4

4 Conclusions

In this study, the effect of adding different doses of barium hydroxide on the performance of CGBM specimen in acid mine water with sulfate ions was explored. And the experimental results including the mass, UPV, compressive strength, as well as the relationship between compressive strength and UPV were determined. According to the results obtained, the following conclusions can be drawn:

- (1) The changes of mass, UPV and compressive strength of CGBM specimens with barium hydroxide in sulfuric acid solution were basically similar to each other. Additionally, the exponential relationship between compressive strength and UPV is established based on the experimental results, and a good correlation was observed between compressive strength and UPV results.
- (2) 2.0 kg/m^3 barium hydroxide was the best dosage to improve the mechanical properties of CGBM in acid mine water with sulfate ions. Moreover, with the increase of acidity of the sulfuric acid solution, the degradation degree of mechanical properties would increase.

- (3) The results of SEM and XRD show that the content of corrosion products such as ettringite, and gypsum in the specimens with barium hydroxide was lower than that in the control specimens, and the internal structure was more complete.
- (4) The calcium silicate hydrate, ettringite and dihydrate gypsum were generated in the early age (0–180 days) would fill the pores in CGBM specimens and improved the mechanical properties. However, in the late age (180–270 days), the calcium silicate hydrate was dissolved and the dihydrate gypsum expanded, resulting in the decline of mechanical properties.

Acknowledgement: The authors gratefully acknowledge the financial support of the National Natural Science Foundation of China (Grant No. 51974192), the Distinguished Youth Funds of National Natural Science Foundation of China (Grant No. 51925402), and Shanxi-Zheda Institute of Advanced Materials and Chemical Engineering Project (2021SX-TD001).

Funding Statement: This study was sponsored by the National Natural Science Foundation of China (Grant No. 51974192), the Distinguished Youth Funds of National Natural Science Foundation of China (Grant No. 51925402), and Shanxi-Zheda Institute of Advanced Materials and Chemical Engineering Project (2021SX-TD001).

Conflicts of Interest: The authors declare that they have no conflicts of interest to report regarding the present study.

References

1. Guo, Y. X., Zhao, Y. H., Wang, S. W., Feng, G. R., Zhang, Y. J. et al. (2021). Stress-strain-acoustic responses in failure process of coal rock with different height to diameter ratios under uniaxial compression. *Journal of Central South University*, 28(6), 1724–1736. DOI 10.1007/s11771-021-4729-3.
2. Xu, H., Du, H., Kang, L., Cheng, Q., Feng, D. et al. (2021). Constructing straight pores and improving mechanical properties of GanguBased porous ceramics. *Journal of Renewable Materials*, 9(12), 2129–2141. DOI 10.32604/jrm.2021.016090.
3. Gao, S., Zhang, S., Guo, L. (2021). Application of coal gangue as a coarse aggregate in green concrete production: A review. *Materials*, 14(22), 6803. DOI 10.3390/ma14226803.
4. Deng, X. J., Klein, B., Hallbom, D. J., de Wit, B., Zhang, J. X. (2018). Influence of particle size on the basic and time-dependent rheological behaviors of cemented paste backfill. *Journal of Materials Engineering and Performance*, 27(7), 3478–3487. DOI 10.1007/s11665-018-3467-7.
5. Zhu, W., Xu, J., Xu, J., Chen, D., Shi, J. (2017). Pier-column backfill mining technology for controlling surface subsidence. *International Journal of Rock Mechanics and Mining Sciences*, 96, 58–65. DOI 10.1016/j.ijrmms.2017.04.014.
6. Feng, G. R., Du, X. J., Guo, Y. X., Qi, T. Y., Wang, Z. H. et al. (2019). Basic theory of constructional backfill mining and the underground space utilization concept. *Journal of China Coal Society*, 44(1), 74–84. DOI 10.13225/j.cnki.jccs.2018.1598.
7. Xu, J. L., Xuan, D. Y., Zhu, W. B., Xiao, X. Z., Tenng, H. (2015). Study and application of coal mining with partial backfilling. *Journal of China Coal Society*, 40(6), 1303–1312. DOI 10.13225/j.cnki.jccs.2015.3055.
8. Zhang, X. N. (2017). Harm and prevention measures of acid mine water in coal mine. *Shanxi Chemical Industry*, 37(5), 150–157. DOI 10.16525/j.cnki.cn14-1109/tq.2017.05.48.
9. Dong, L., Gao, Q., Nan, S. Q., Du, J. Q. (2013). Performance and hydration mechanism of new super fine cemented whole-tailings backfilling materials. *Journal of Central South University (Science and Technology)*, 44(4), 1571–1577.
10. Rozière, E., Loukili, A., Hachem, R. E., Grondin, F. (2009). Durability of concrete exposed to leaching and external sulphate attacks. *Cement and Concrete Research*, 39(12), 1188–1198. DOI 10.1016/j.cemconres.2009.07.021.

11. Bondar, D., Nanukuttan, S. (2022). External sulphate attack on alkali-activated slag and slag/fly ash concrete. *Buildings*, 12(2), 94. DOI 10.3390/buildings12020094.
12. Xiao, J., Qu, W. J., Zhu, P., Tian, J. B. (2017). Experimental study of interface shear behaviors between sand and concrete corroded by sulfuric acid. *Rock and Soil Mechanics*, 38(9), 2613–2619. DOI 10.16285/j.rsm.2017.09.019.
13. Zhao, L., Liu, J. H., Ji, H. G. (2017). Performance improvement and mechanism of concrete with the addition of barium hydroxide reagent in typical sulfate environment. *Journal of China Coal Society*, 42(7), 1732–1739. DOI 10.13225/j.cnki.jccs.2016.1521.
14. Sun, X., Li, T., Shi, F., Liu, X., Zong, Y. et al. (2022). Sulphate corrosion mechanism of ultra-high-performance concrete (UHPC) prepared with seawater and sea sand. *Polymers*, 14(5), 971. DOI 10.3390/polym14050971.
15. Wang, K., Guo, J., Yang, L. (2021). Effect of Dry–Wet ratio on sulfate transport-reaction mechanism in concrete. *Construction and Building Materials*, 302, 124418. DOI 10.1016/j.conbuildmat.2021.124418.
16. He, R., Zheng, S., Gan, V. J. L., Wang, Z., Fang, J. et al. (2020). Damage mechanism and interfacial transition zone characteristics of concrete under sulfate erosion and dry-wet cycles. *Construction and Building Materials*, 255, 119340. DOI 10.1016/j.conbuildmat.2020.119340.
17. Zhao, G., Li, J., Shi, M., Fan, H., Cui, J. et al. (2020). Degradation mechanisms of cast-in-situ concrete subjected to internal-external combined sulfate attack. *Construction and Building Materials*, 248, 118683. DOI 10.1016/j.conbuildmat.2020.118683.
18. Mahdikhani, M., Bamshad, O., Shirvani, M. F. (2018). Mechanical properties and durability of concrete specimens containing nano silica in sulfuric acid rain condition. *Construction and Building Materials*, 167, 929–935. DOI 10.1016/j.conbuildmat.2018.01.137.
19. Nematzadeh, M., Fallah-Valukolae, S. (2017). Erosion resistance of high-strength concrete containing forta-ferro fibers against sulfuric acid attack with an optimum design. *Construction and Building Materials*, 154, 675–686. DOI 10.1016/j.conbuildmat.2017.07.180.
20. Hasan-Nattaj, F., Nematzadeh, M. (2017). The effect of forta-ferro and steel fibers on mechanical properties of high-strength concrete with and without silica fume and nano-silica. *Construction and Building Materials*, 137, 557–572. DOI 10.1016/j.conbuildmat.2017.01.078.
21. Siad, H., Mesbah, H. A., Khelafi, H., Kamali-Bernard, S., Mouli, M. (2010). Effect of mineral admixture on resistance to sulphuric and hydrochloric acid attacks in self-compacting concrete. *Canadian Journal of Civil Engineering*, 37(3), 441–449. DOI 10.1139/L09-157.
22. Araghi, H. J., Nikbin, I. M., Reskati, S. R. E., Allahyari, H. (2015). An experimental investigation on the erosion resistance of concrete containing various PET particles percentages against sulfuric acid attack. *Construction and Building Materials*, 77, 461–471. DOI 10.1016/j.conbuildmat.2014.12.037.
23. Chen, Q., Tao, Y., Feng, Y., Zhang, Q., Liu, Y. (2021). Utilization of modified copper slag activated by Na₂SO₄ and CaO for unclassified lead/Zinc mine tailings based cemented paste backfill. *Journal of Environmental Management*, 290, 112608. DOI 10.1016/j.jenvman.2021.112608.
24. Xin, J., Liu, L., Xu, L., Wang, J., Yang, P. et al. (2022). A preliminary study of aeolian sand-cement-modified gasification slag-paste backfill: Fluidity, microstructure, and leaching risks. *Science of the Total Environment*, 830, 154766. DOI 10.1016/j.scitotenv.2022.154766.
25. Yang, K., Sim, J., Nam, S. (2010). Enhancement of reactivity of calcium hydroxide-activated slag mortars by the addition of barium hydroxide. *Construction and Building Materials*, 24(3), 241–251. DOI 10.1016/j.conbuildmat.2009.09.001.
26. Mobasher, N., Bernal, S. A., Hussain, O. H., Apperley, D. C., Kinoshita, H. et al. (2014). Characterisation of Ba(OH)₂–Na₂SO₄–Blast furnace slag cement-like composites for the immobilisation of sulfate bearing nuclear wastes. *Cement and Concrete Research*, 66, 64–74. DOI 10.1016/j.cemconres.2014.07.006.
27. Wang, C., Kong, M. R. F., Pan, L. S. (2021). Effects of polycarboxylate superplasticizers with different side-chain lengths on the resistance of concrete to chloride penetration and sulfate attack. *Journal of Building Engineering*, 43, 102817. DOI 10.1016/j.job.2021.102817.

28. García-Vera, V. E., Tenza-Abril, A. J., Saval, J. M., Lanzón, M. (2018). Influence of crystalline admixtures on the short-term behaviour of mortars exposed to sulphuric acid. *Materials*, 12(1), 82. DOI 10.3390/ma12010082.
29. Ran, H. Y., Guo, Y. X., Feng, G. R., Qi, T. Y., Du, X. J. (2021). Creep properties and resistivity-ultrasonic-AE responses of cemented gangue backfill column under high-stress area. *International Journal of Mining Science and Technology*, 31(3), 401–412. DOI 10.1016/j.ijmst.2021.01.008.
30. Guo, Y. X., Ran, H. Y., Feng, G. R., Du, X. J., Zhao, Y. H. et al. (2022). Deformation and instability properties of cemented gangue backfill column under step-by-step load in constructional backfill mining. *Environmental Science and Pollution Research*, 29(2), 2325–2341. DOI 10.1007/s11356-021-15638-z.
31. Guo, Y. X., Zhao, Y. H., Feng, G. R., Ran, H. Y., Zhang, Y. J. (2021). Study on damage size effect of cemented gangue backfill body under uniaxial compression. *Chinese Journal of Rock Mechanics and Engineering*, 40(12), 2434–2443. DOI 10.13722/j.cnki.jrme.2021.0527.
32. ASTM C192/C192M (2016). Standard Practice for Making and Curing Concrete Test Specimens in the Laboratory. USA: American Society for Testing and Materials International. DOI 10.1520/C0192_C0192M-16.
33. Kumar, R., Verma, M., Dev, N. (2021). Investigation on the effect of seawater condition, sulphate attack, acid attack, freeze–thaw condition, and wetting–drying on the geopolymer concrete. *Iranian Journal of Science and Technology, Transactions of Civil Engineering*, DOI 10.1007/s40996-021-00767-9.
34. Khan, S. R. M., Noorzai, J., Kadir, M. R. A., Waleed, A. M. T., Jaafar, M. S. (2007). UPV method for strength detection of high performance concrete. *Structural Survey*, 25(1), 61–73. DOI 10.1108/02630800710740985.
35. Shi, M., Jeong, D. H., Lee, S. W., Choi, Y. (2018). Relationship between UPV and strength of rubber-concrete. *Defect and Diffusion Forum*, 382, 225–229. DOI 10.4028/www.scientific.net/DDF.382.225.
36. Chiriatti, L., François, P., Mercado-Mendoza, H., Apedo, K. L., Fond, C. et al. (2020). Monitoring of the rebar-concrete bond structural health through ultrasonic measurements: Application to recycled aggregate concrete. *Journal of Civil Structural Health Monitoring*, 10(4), 595–607. DOI 10.1007/s13349-020-00404-5.
37. Mohammed, T. U., Rahman, M. N. (2016). Effect of types of aggregate and sand-to-aggregate volume ratio on UPV in concrete. *Construction and Building Materials*, 125, 832–841. DOI 10.1016/j.conbuildmat.2016.08.102.
38. Marie, I. (2016). Zones of weakness of rubberized concrete behavior using the UPV. *Journal of Cleaner Production*, 116, 217–222. DOI 10.1016/j.jclepro.2015.12.096.
39. Pang, J. Y., Su, Q., Wang, Y., Jiang, P. W., Zhang, Q. (2021). Mechanical properties of basalt fiber concrete under sulfate erosion. *China Science Paper*, 16(12), 1361–1365. DOI 10.3969/j.issn.2095-2783.2021.12.015.
40. Xiao, D. W., Zhen, Y. Z., Yu, L. C., Lei, F., Tian, H. Q. (2018). Impact and improvement of crushed tuff sand on sulfate resistance of cement concrete at Low temperature. *American Society of Civil Engineers*, 30(10), 1–8. DOI 10.1061/(ASCE)MT.1943-5533.0002457.
41. Jeong, Y., Yum, W. S., Jeon, D., Oh, J. E. (2017). Strength development and microstructural characteristics of barium hydroxide-activated ground granulated blast furnace slag. *Cement and Concrete Composites*, 79, 34–44. DOI 10.1016/j.cemconcomp.2017.01.013.
42. Madandoust, R., Ghavidel, R., Nariman-Zadeh, N. (2010). Evolutionary design of generalized GMDH-type neural network for prediction of concrete compressive strength using UPV. *Computational Materials Science*, 49(3), 556–567. DOI 10.1016/j.commatsci.2010.05.050.
43. Yoshida, M., Asano, M., Suwa, T., Reber, N., Spohr, R. et al. (1997). Creation of thermo-responsive ion-track membranes. *Advanced Materials*, 9(9), 757–758. DOI 10.1002/adma.19970090917.
44. Bogas, J. A., Gomes, M. G., Gomes, A. (2013). Compressive strength evaluation of structural lightweight concrete by non-destructive ultrasonic pulse velocity method. *Ultrasonics*, 53(5), 962–972. DOI 10.1016/j.ultras.2012.12.012.
45. Karatasios, I., Kilikoglou, V., Theoulakis, P., Colston, B., Watt, D. (2008). Sulphate resistance of lime-based barium mortars. *Cement and Concrete Composites*, 30(9), 815–821. DOI 10.1016/j.cemconcomp.2008.06.010.
46. Liu, J. H., Gao, M., Wu, A. X. (2016). Corrosion and deterioration mechanism of water-rich filling materials in acid solution. *Chinese Journal of Engineering*, 38(9), 1212–1220. DOI 10.13374/j.issn2095-9389.2016.09.003.
47. Bai, H., Li, Y., Dai, D. (2022). Study on the durability of recycled powder concrete against sulfate attack under partial immersion condition. *Journal of Renewable Materials*, 10(6), 1–20. DOI 10.32604/jrm.2022.020148.